

Controlled Processing  
of Nanoparticle-Based  
Materials and  
Nanostructured Films

---

---

COPYRIGHTED MATERIAL



## EFFECT OF FOCUSED ION BEAM PATTERNING ON ENLARGING ANODIZATION WINDOW AND INTERPORE DISTANCE FOR ORDERED POROUS ANODIC ALUMINA

Bo Chen, Kathy Lu, Zhipeng Tian

Materials Science and Engineering, Virginia Polytechnic Institute and State University  
Blacksburg, Virginia 24061, USA

### ABSTRACT

Highly ordered porous anodic alumina with alternating-sized pores and in hexagonal and square arrangements has been produced with focused ion beam patterning guided anodization. Deeper focused ion beam patterned concaves induce better developed pores during the anodization. Focused ion beam patterning also effectively enlarges the anodization window; ordered alternating-sized nanopore arrangement and square arrangement with 150 nm interpore distance can be produced at 40-80 V potentials. Under the guidance of FIB patterned concaves in Moiré patterns, different alumina nanopore arrays in Moiré patterns can be obtained after the anodization.

### INTRODUCTION

In recent years, nanomaterials have attracted great interest due to their unique electronic, magnetic, and optoelectronic properties and a broad range of applications in new nano-devices.<sup>1-8</sup> Among different fabrication methods of nanomaterials, templating based on porous anodic alumina has the advantage of offering uniform diameter and controlled aspect ratio pores, which can then be used to create high density and perfectly vertical nanorod and nanowire arrays.

Self-organized porous anodic alumina cannot provide highly ordered nanopores across large areas, the honeycomb-like structure is limited in only several micrometer scale. Even though two-step anodization process can increase the area of highly ordered nanopore arrays, the anodization condition is limited in a narrow window: 63 nm (0.3 M sulfuric acid, 25 V),<sup>9-11</sup> 100 nm (0.3 M oxalic acid, 40 V),<sup>12-13</sup> 500 nm (0.3M phosphoric acid, 195 V),<sup>14-15</sup> and only hexagonal arrangement of uniform diameter pores can be produced. Attempts to fabricate porous anodic alumina with arrangement other than hexagon and with different pore diameter have been made. Square arrangement of square nanopores was synthesized using nano-indentation.<sup>16-18</sup> Similarly, triangular anodic alumina nanopores with a graphite lattice structure were synthesized with the guidance of nano-indented graphite lattice structure concaves.<sup>19</sup> With the guidance of the focused ion beam created gradient- and alternating-sized concave patterns, hexagonally ordered gradient- and alternating-sized nanopore arrays were produced.<sup>20</sup> Moreover, Y-branched anodic alumina oxide channels were first fabricated by reducing the anodization voltage by a factor of  $1/\sqrt{2}$ .<sup>21</sup> Similarly, after primary stem pores were fabricated by a typical two-step anodization process, n-branched nanopores were created by reducing the anodization voltage by a factor of  $1/\sqrt{n}$ .<sup>22-24</sup> Moreover, tree-like nanopore arrays were obtained by further reducing the anodization voltage by a factor of  $1/\sqrt{m}$  to generate the third layer of the branched pores at the bottom of the second layer of branched pores. All the interpore distances of the above discussed porous anodic alumina were

determined by the applied voltage with a linear proportional constant of 2.5 nm/V.<sup>15</sup> More work is needed to make porous anodic alumina with different interpore distances under the same anodization condition.

In this study, focused ion beam (FIB) patterned concave arrays are used to guide the growth of alternating-sized diameter and different nanopore arrangement. The effect of FIB guidance on enlarging the anodization window is examined. Anodization of Moiré patterns with different interpore distance is also studied in order to examine the potential of FIB patterning in fabrication of different interpore distance patterns.

### EXPERIMENTAL PROCEDURE

High purity aluminum foils (99.999%, Goodfellow Corporation, Oakdale, PA) with 8 mm×22 mm×0.3mm size were used as the starting material. After being washed with ethanol and acetone, they were annealed at 500°C for 2 hrs in high purity flowing Ar gas with 5°C/min heating and cooling rates to recrystallize the aluminum foils and remove mechanical stress.

For electropolishing, the annealed aluminum foils were degreased in ethanol and acetone for 5 min, respectively, followed by DI water rinsing after each step. The aluminum foils were then immersed in a 0.5 wt% NaOH solution for 10 min with ultrasound in order to remove the oxidized surface layer. After that, the aluminum foils were electropolished in a 1:4 mixture of perchloric acid (60%-62%): ethanol (95%) (volume ratio) under a constant voltage of 12 V at room temperature with 500 rps stirring speed for 5 min.

A dual beam focused Ga<sup>+</sup> ion beam microscope (FIB, FEI Helios 600 Nano Lab, Hillsboro, OR) was employed to create different concave patterns to guide the anodization. The accelerating voltage for the FIB microscope was 30 keV. The beam diameter was ~30 nm. The beam current was 28 pA. The beam dwell time at each scan was 3 μs. The FIB created patterns were observed in the SEM mode, which allowed for in-situ monitoring of the surface features of the Al foils at different stages of the ion exposure.

The FIB patterned Al foils were anodized in 0.3 M oxalic acid at 40-60 V and 0°C for 30 min, and in 0.05 M oxalic acid at 80 V and 0°C for 30 min. For the Moiré pattern, the FIB patterned Al foils were anodized in 0.3 M phosphoric acid under 20 mA constant current at 0°C for 5 min. The voltage was ~140 V after a few seconds of anodization. Pore opening was carried out in 5 wt% phosphoric acid at 30°C for 10 min. The porous anodic alumina patterns were characterized by scanning electron microscopy (Quanta 600 FEG, FEI Company, Hillsboro, OR).

### RESULTS AND DISCUSSION

#### FIB exposure time effect

Figure 1 shows anodized alternating diameter nanopores with different FIB patterning exposure time. The interpore distance is 125 nm. After the anodization, the pore sizes increase with the FIB exposure time even through the anodization condition is the same. When the FIB exposure time is only 1 s with the dwell time at 1 μs, both large and small FIB concaves are very

shallow, less than 3 nm. The diameters of the small and large concaves are 30 nm and 65 nm, respectively. After the anodization (Figure 1(a)), the small concaves induce small anodized nanopores with 30 nm diameter. The large concaves induce large nanopores with 40 nm diameter, but the pore shape is not well defined. The nanopore arrangement maintains the pre-defined hexagonal pattern. When the FIB exposure time increases, the depth and the diameters of the concave patterns increase. For example, after 15 s of the FIB patterning, the small pores have 8 nm depth and 45 nm diameter, and the large pores have 50 nm depth and 80 nm diameter. As a result, the diameters of the anodized nanopores increase and the shapes of the anodized nanopores become much more round. When the FIB patterning time is 6 s and 15 s (Figures 1(b) and 1(c)), the anodized large nanopore sizes are 70 nm and 90 nm, respectively, and the anodized small pore sizes are 35 nm and 45 nm, respectively. At the same time, the anodized nanopores with different FIB exposure time maintain the ordered hexagonal arrangement. When the FIB time is 80 s (Figure 1(d)), the large and small anodized nanopore diameters are 90 nm and 65 nm, respectively.

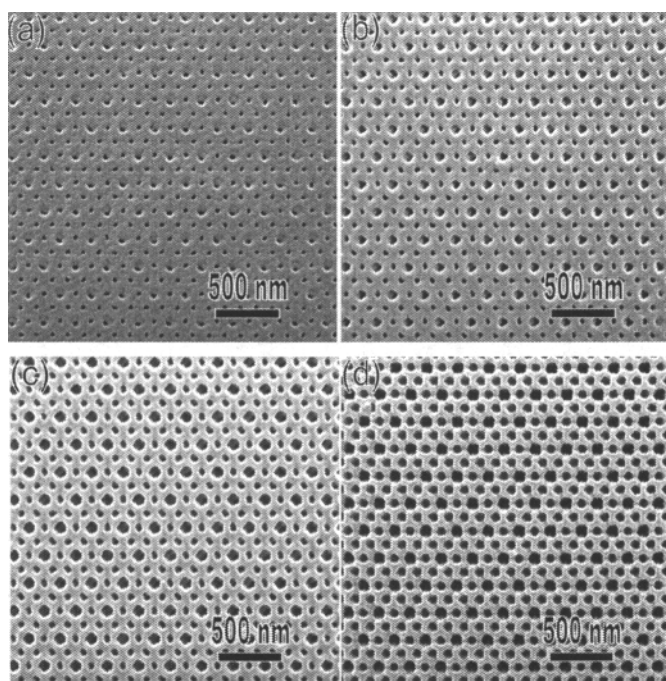


Figure 1. SEM images of anodized nanopore pattern with different FIB exposure time: (a) 1 s, (b) 6 s, (c) 15 s, (d) 80 s.

The effect of the FIB exposure time is directly related to the concave size and shape. When the FIB patterning time is short, the concaves are very shallow (Figure 1(a)), and the curvature of

the concave is very large, which results in a small electrical field at the bottoms of the concaves during the anodization. The concaves cannot effectively guide the subsequent anodization; the anodized nanopores grow slowly and the pore shape is less defined. However, the  $\text{Ga}^+$  implantation and aluminum amorphization at the concave circumferences are effective enough in maintaining the pore pattern in the hexagonal arrangement. As the FIB exposure time increases, the patterned concaves grow larger and deeper (Figures 1(b) and 1(c)), along with more  $\text{Ga}^+$  implantation and aluminum amorphization. As a result, the anodized pores have larger diameters and more round pore shapes.

For different FIB exposure time, the pristine Al surfaces among the concaves are also different. When the FIB exposure time is short (Figures 1(a), 1(b), 1(c)), there is an un-anodized triangular aluminum pillar at the junction of a large concave and two adjoining small concaves. During the anodization, these pillars act as the effective electrical circuit to anodize nearby aluminum. Because of the asymmetric nature of the electric field, the pores are not round. The small pores elongate in the direction of the junction. As the FIB exposure time increases further (Figure 1(d)), the pristine surface after the FIB exposure diminishes/disappears, and the FIB patterning effect on the pore shape becomes less obvious or disappears. As a result, both the large and small anodized pores in Figure 1(d) are round.

### Anodization voltage effect

FIB patterning also enlarges the anodization window for ordered nanopore pattern and different nanopore arrangement. Two different arrangements are studied here. The first is alternating-sized nanopores in hexagonal arrangement, and the second is uniform-sized nanopores in square arrangement. The same FIB patterned concave arrays with 150 nm interpore distance are anodized at three different conditions: 0.3 M oxalic acid at 40 V, 0.3 M oxalic acid at 60 V, and 0.05 M oxalic acid at 80 V. The SEM images of the nanopores after the anodization are shown in Figure 2. Pore widening was not undertaken on these samples and the images are the pristine structure after the anodization. As shown in Figures 2(a), 2(c), and 2(e), all these samples keep growing alternating diameter nanopores in hexagonal arrangement. As shown in Figures 2(b), 2(d), and 2(f), all the samples keep growing uniform diameter nanopores in square arrangement. However, under the traditional self-organized anodization condition, both ordered square nanopore arrangement and alternating diameter nanopores are difficult to obtain. Because the interpore distance is linearly proportional to the applied voltage with a constant of 2.5 nm/V, even with the guidance of the FIB patterning, the ordered alternating diameter and square nanopore arrangement with 150 nm interpore distance can only be synthesized at 60 V applied potential. In this study, with the FIB patterning, ordered nanopore arrangement can be anodized in the potential range of 40-80 V, which means deep concaves,  $\text{Ga}^+$  implantation, and the re-deposition of amorphous aluminum in combination play a significant role in the nanopore growth. The FIB guidance enlarges the anodization window for obtaining the ordered nanopore arrangement.

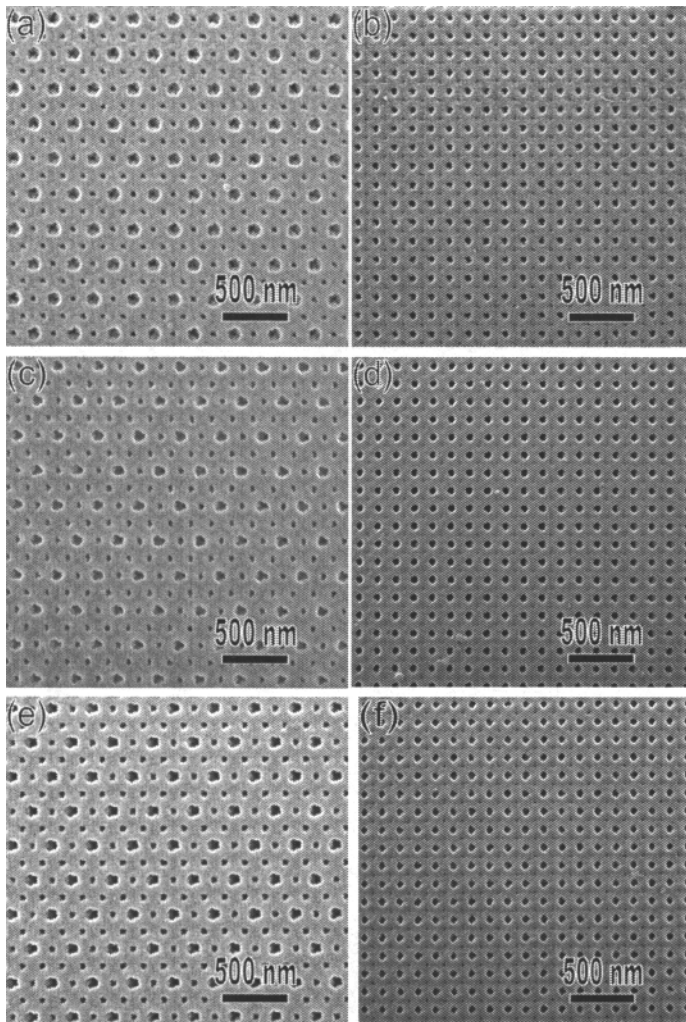


Figure 2. SEM images of anodized nanopore patterns with the same FIB pattern but different anodization condition: (a) and (b) 0.3 M oxalic acid under 40 V and 0°C for 30 min, (c) and (d) 0.3 M oxalic acid under 60 V and 0°C for 30 min, (e) and (f) 0.05 M oxalic acid under 80 V and 0°C for 30 min. The FIB pattern of (a), (c), and (e) is alternating-sized concave pattern with 150 nm inter-pore distance. The FIB pattern of (b), (d), and (f) is uniform concaves in square arrangement with 150 nm inter-pore distance.

### Moiré pattern

Moiré patterns are the composite patterns created by the superposition of two identical patterns with a rotation angle, or by superposition of two different patterns with a rotation angle. There are many different intercore distances in the Moiré pattern. Since the intercore distance is dependent on the applied voltage with a linear proportional constant of 2.5 nm/V, the Moiré pattern cannot be synthesized by the conventional self-organized anodization. From the previous discussion, FIB patterning shows great potential in enlarging the anodization window and maintaining the ordered nanopore arrangement. In this section, Moiré nanopore patterns with different intercore distances are studied at a certain voltage potential.

Figure 3 shows the SEM images of anodized porous alumina arrays with graphite lattice structure Moiré patterns. The FIB patterned concave arrays are created by the superposition of two graphite lattice structure concave patterns with identical intercore distance and rotation angle of  $\alpha$ . The intercore distance of the graphite lattice structure concave arrays is 350 nm, and the rotation angle  $\alpha$  is (a) 5°, (b) 10°, (c) 20°, (d) 30°, respectively. After the anodization, porous alumina arrays with various Moiré patterns are obtained; the periodicity of the Moiré patterns is: (a) 6.74  $\mu\text{m}$ , (b) 3.67  $\mu\text{m}$ , (c) 1.60  $\mu\text{m}$ , (d) 1.14  $\mu\text{m}$ , respectively.

According to the fundamental theory of Moiré patterns<sup>25-28</sup>, the periodicity  $D$  of the Moiré patterns depends on the lattice constant of both layers ( $d_1$  and  $d_2$ ) and the rotation angle  $\alpha$ . The spectral approach, which is based on the Fourier theory, is used to analyze the Moiré phenomena. For the Moiré pattern created by the superposition of two hexagonal concave patterns with different lattice and with the rotation angle of  $\alpha$ , the periodicity of the Moiré pattern is:

$$D = \frac{d_1 d_2}{\sqrt{d_1^2 + d_2^2 - 2d_1 d_2 \cos \alpha}} \quad (1)$$

When  $d_1 = d_2$ , the equation can be further simplified into:

$$D = \frac{d}{2 \sin(\alpha/2)} \quad (2)$$

The graphite lattice structure pattern can be considered as hexagonal pattern, as shown in Figure 4(b), and the intercore distance is  $\sqrt{3}$  times of the original value. According to the spectral approach, the multiplication intensity of the resulting image is:  $I(x,y) = I_1(x,y) \cdot I_2(x,y)$  in the direct space. The Moiré pattern periodicity is the distance of the two neighboring spectrum maximum. In the new hexagonal pattern, only half of the triangular gravity centers exist, such as a, b, and c in Figure 4(b). Therefore, in the direct space of Moiré pattern, the intensities of the spectrum at a, b, and c are just  $I(x,y) = I_1(x,y)$ , and it will not be the maximum of the resulting image. As a result, for the periodicity of the graphite lattice structure Moiré pattern in Figure 3,  $d_1' = d_2' = \sqrt{3}d$ , and  $D = \frac{\sqrt{3}d}{2 \sin(\alpha/2)}$ . From this equation, the periodicities of the Moiré patterns of Figures 3(a)-(d) are



calculated as 6.95  $\mu\text{m}$ , 3.48  $\mu\text{m}$ , 1.75  $\mu\text{m}$ , and 1.17  $\mu\text{m}$ , respectively. The experimentally observed periodicities are in good agreement with the theoretical value.

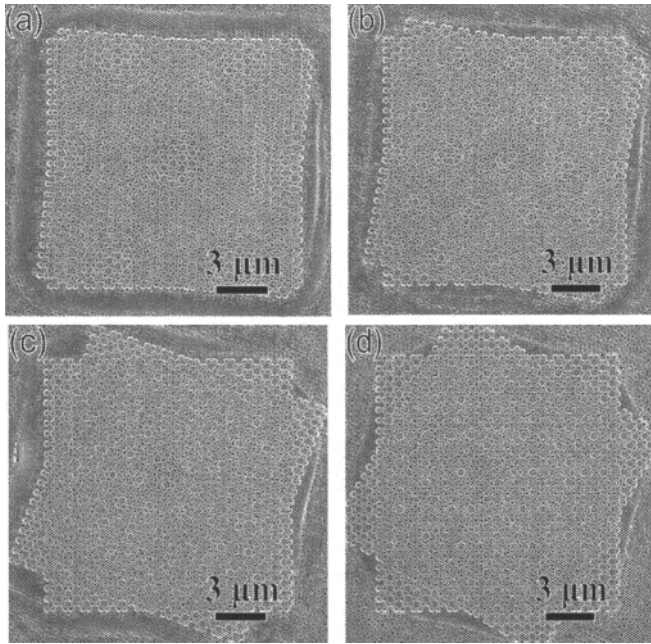


Figure 3. SEM images of porous alumina arrays with graphite lattice structure Moiré pattern. The patterns are formed by anodization of aluminum with superimposition of two identical FIB patterned graphite lattice structure concaves, the interpore distance is 350 nm, and the rotation angle between the FIB patterns is: (a) 5°, (b) 10°, (c) 20°, (d) 30°.

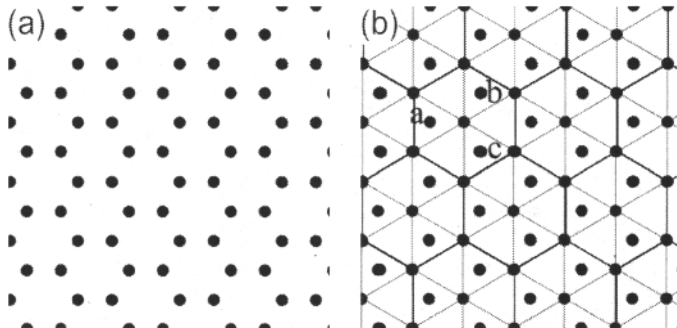


Figure 4. Schematic drawing of (a) graphite lattice structure nanopore arrangement, (b) different

view of the same graphite lattice structure arrangement as hexagonal arrangement with three points in the hexagon.

## CONCLUSIONS

With the guidance of the FIB patterned concave arrays, alternating diameter nanopore arrangement is obtained. When the depth of the FIB patterned concaves is shallow, the diameter difference of the alternating diameter nanopores is not obvious. The deeper the FIB patterned concaves, the better developed the alternating diameter nanopore arrays are. The anodization window of ordered alternating diameter nanopore arrangement and square nanopore arrangement with 150 interpore distance is enlarged to 40-80 V thanks to the guidance of the FIB patterned concave arrays. This guiding effect also enables the creation of patterns with different interpore distances under the same anodization condition. Moiré pattern with various interpore distance and periodicity are obtained.

## ACKNOWLEDGEMENT

The authors acknowledge the financial support from National Science Foundation under grant No. CMMI-0824741 and the Institute for Critical Technology and Applied Science of Virginia Tech. Assistance from John McIntosh and Stephen McCartney from the Nanoscale Characterization and Fabrication Laboratory of Virginia Tech is greatly acknowledged.

## REFERENCES

- <sup>1</sup>Y. Q. Wang, Y. M. Sun, and K. Li, Dye-Sensitized Solar Cells Based on Oriented ZnO Nanowire-Covered TiO<sub>2</sub> Nanoparticle Composite Film Electrodes, *Mater. Lett.*, **63**, 1102-1104 (2009).
- <sup>2</sup>T. S. Kang, A. P. Smith, B. E. Taylor, and M. F. Durstock, Fabrication of Highly-Ordered TiO<sub>2</sub> Nanotube Arrays and Their Use in Dye-Sensitized Solar Cells, *Nano Lett.*, **9**, 601-606 (2009).
- <sup>3</sup>D. I. Suh, S. Y. Lee, T. H. Kim, J. M. Chun, E. K. Suh, O. B. Yang, and S. K. Lee, The Fabrication and Characterization of Dye-Sensitized Solar Cells with a Branched Structure of ZnO Nanowires, *Chem. Phys. Lett.*, **442**, 348-353 (2007).
- <sup>4</sup>J. Hahn, and C. M. Lieber, Direct Ultrasensitive Electrical Detection of DNA and DNA Sequence Variations Using Nanowire Nanosensors, *Nano Lett.*, **4**, 51-54 (2004).
- <sup>5</sup>A. K. Wanekaya, W. Chen, N. V. Myung, and A. Mulchandani, Nanowire-Based Electrochemical Biosensors, *Electroanal.*, **18**, 533-550 (2006).
- <sup>6</sup>Y. Cui, Q. Q. Wei, H. K. Park, and C. M. Lieber, Nanowire Nanosensors for Highly Sensitive and Selective Detection of Biological and Chemical Species, *Science*, **293**, 1289-1292 (2001).
- <sup>7</sup>C. K. Chan, H. L. Peng, G. Liu, K. McIlwrath, X. F. Zhang, R. A. Huggins, and Y. Cui, High-Performance Lithium Battery Anodes Using Silicon Nanowires, *Nat. Nanotech.*, **3**, 31-35 (2008).
- <sup>8</sup>K. Q. Peng, J. S. Jie, W. J. Zhang, and S. T. Lee, Silicon Nanowires for Rechargeable Lithium-Ion Battery Anodes, *Appl. Phys. Lett.*, **93**, 033105-1 (2008).
- <sup>9</sup>H. Asoh, K. Nishio, M. Nakao, A. Yokoo, T. Tamamura, and H. Masuda, Fabrication of Ideally Ordered Anodic Porous Alumina with 63 nm Hole Periodicity Using Sulfuric Acid, *J. Vac. Sci. Technol. B*, **19**, 569-572 (2001).
- <sup>10</sup>H. Masuda, F. Hasegawa, and S. Ono, Self-Ordering of Cell Arrangement of Anodic Porous

Alumina Formed in Sulfuric Acid Solution, *J. Electrochem. Soc.*, **144**, L127-L130 (1997).

<sup>11</sup>A. P. Li, F. Muller, A. Birner, K. Nielsch, and U. Gosele, Hexagonal Pore Arrays with a 50-420 nm Interpore Distance Formed by Self-Organization in Anodic Alumina, *J. Appl. Phys.*, **84**, 6023-6026 (1998).

<sup>12</sup>F. Y. Li, L. Zhang, and R. M. Metzger, On the Growth of Highly Ordered Pores in Anodized Aluminum Oxide, *Chem. Mater.*, **10**, 2470-2480 (1998).

<sup>13</sup>H. Masuda and K. Fukuda, Ordered Metal Nanohole Arrays Made by a Two-Step Replication of Honeycomb Structures of Anodic Alumina, *Science*, **268**, 1466-1468 (1995).

<sup>14</sup>H. Masuda, K. Yada, and A. Osaka, Self-Ordering of Cell Configuration of Anodic Porous Alumina with Large-Size Pores in Phosphoric Acid Solution. *Jn. J. Appl. Phys. Part 2-Letters*, **37**, L1340-L1342 (1998).

<sup>15</sup>K. Nielsch, J. Choi, K. Schwirn, R. B. Wehrspohn, and U. Gosele, Self-Ordering Regimes of Porous Alumina: The 10% Porosity Rule, *Nano Lett.*, **2**, 677-680 (2002).

<sup>16</sup>H. Asoh, S. Ono, T. Hirose, M. Nakao, and H. Masuda, Growth of Anodic Porous Alumina with Square Cells, *Electrochim. Acta*, **48**, 3171-3174 (2003).

<sup>17</sup>N. Y. Kwon, K. H. Kim, J. Heo, and I. S. Chung, Fabrication of Ordered Anodic Aluminum Oxide with Matrix Arrays of Pores Using Nanoimprint, *J. Vac. Sci. Technol. A*, **27**, 803-807 (2009).

<sup>18</sup>Z. P. Tian, K. Lu, and B. Chen, Unique Nanopore Pattern Formation by Focused Ion Beam Guided Anodization, *Nanotechnology*, accepted.

<sup>19</sup>H. Masuda, H. Asoh, M. Watanabe, K. Nishio, M. Nakao, and T. Tamamura, Square and Triangular Nanohole Array Architectures in Anodic Alumina, *Adv. Mater.* **13**, 189-192 (2001).

<sup>20</sup>B. Chen, K. Lu, and Z. P. Tian, Gradient and Alternating Diameter Nanopore Templates by Focused Ion Beam Guided Anodization, *Electrochim. Acta*, accepted.

<sup>21</sup>J. Li, C. Papadopoulos, and J. Xu, Growing Y-Junction Carbon Nanotubes, *Nature*, **402**, 253-254 (1999).

<sup>22</sup>G. W. Meng, Y. J. Jung, A. Y. Cao, R. Vajtai, and P. M. Ajayan, Controlled Fabrication of Hierarchically Branched Nanopores, Nanotubes, and Nanowires, *Proc. Nat. Acad. Sci.* **102**, 7074 (2005).

<sup>23</sup>S. S. Chen, Z. Y. Ling, X. Hu, and Y. Li, Controlled Growth of Branched Channels by a Factor of  $1/\sqrt{N}$  Anodizing Voltage?, *J. Mater. Chem.*, **19**, 5717-5719 (2009).

<sup>24</sup>J. P. Zhang, C. S. Dayb, and D. L. Carroll, Controlled Growth of Novel Hyper-Branched Nanostructures in Nanoporous Alumina Membrane, *Chem. Commun.*, **45**, 6937-6939 (2009).

<sup>25</sup>J. Choi, R. B. Wehrspohn, and U. Gösele, Moiré Pattern Formation on Porous Alumina Arrays Using Nanoimprint Lithography, *Adv. Mater.*, **15**, 1531-1534 (2003).

<sup>26</sup>V. Luchnikov, A. Kondyurin, P. Formanek, H. Lichte, and M. Stamm, Moiré Patterns in Superimposed Nanoporous Thin Films Derived from Block-Copolymer Assemblies, *Nano Lett.*, **7**, 3628-3632 (2007).

<sup>27</sup>I. Amidror, Moiré Patterns Between Aperiodic Layers: Quantitative Analysis and Synthesis, *J. Opt. Soc. Am. A*, **20**, 1900-1919 (2003).

<sup>28</sup>I. Amidror, The Theory of the Moiré Phenomenon, Kluwer Academic Publisher:Norwell, MA, (2000).

